Monday, October 13, 2003
Afternoon Session I
THE NATURE AND EVOLUTION OF THE SEASONAL POLAR CAPS *(Continued)*
1:30 p.m. Victoria Room

Zuber M. T. * Smith D. E. [INVITED]
Observations of the Seasonal Polar Icecaps of Mars at 1064 nm **[#8032]**

Prettyman T. H. * Feldman W. C. Murphy J. R. Funsten H. O. Lawrence D. J. Linn R. R. Maurice S. Tokar R. L.
Seasonal Advance and Retreat of Mars' South Polar Cap as Measured by the Mars Odyssey Neutron Spectrometer **[#8099]**

Calvin W. M. * Titus T. N. Mahoney S. A.
Constraints on the Within Season and Between Year Variability of the North Residual Cap from MGS-TES **[#8036]**

Titus T. N. * Kieffer H. H. Plaut J. J. Christensen P. R. Ivanov A. B. THEMIS Science Team
South Polar Cryptic Region Revisited: THEMIS Observations **[#8081]**

Kieffer H. H. * [INVITED]
Behavior of Solid CO_2 on Mars: Still a Zoo **[#8083]**

Hansen G. B. *
Evolution of Low-Emissivity Spots in the Martian Winter Polar Caps: Mobility of Dust Grains **[#8103]**

GENERAL DISCUSSION

3:30 – 3:45 p.m. BREAK

OBSERVATIONS OF THE SEASONAL POLAR ICECAPS OF MARS AT 1064 nm.
Maria T. Zuber[1] and David E. Smith[2], [1]Dept of Earth Atmospheric and Planetary Sciences, Massachusetts Institute of Technology, 77 Massachusetts Ave. 54-918, Cambridge, MA 02139-4307, e-mail: zuber@mit.edu, [2]Laboratory for Terrestrial Physics, NASA Goddard Space Flight Center, Greenbelt, MD 20771, e-mail: David.E.Smith@nasa.gov.

Introduction. The Mars Orbiter Laser Altimeter (MOLA) [1, 2] is routinely making radiometric observations of Mars at a wavelength of 1064 nm. Although the altimeter function is no longer operational, the MOLA detector [3] continues to measure the reflectivity of the surface. Observations have been obtained almost continuously since the beginning of the Mars Global Surveyor (MGS) [4] mapping mission in February 1999, and are providing measurements relevant to understanding the seasonal cycling of CO_2 surface frost.

Radiometer Data. The field of view of the MOLA detector is approximately 800 μrad and from an altitude of 400 km receives reflected solar radiation from a roughly circular spot ~300 m in diameter. The data are acquired at a rate of 8 Hz and with a ground track velocity of the spacecraft of about 3 km s^{-1} the along-track resolution is slightly less than 400 m, thus providing an almost continuous profiling measurement of Martian surface brightness.

To determine reflectivity, the received optical power can be estimated by a mathematical model that utilizes the MOLA threshold setting and noise counts [5, 6]. Utilizing the link equation [7], observations are normalized to a constant mean solar flux assuming Lambertian scattering to yield a spectral radiance *(I/F)*.

For the purposes of this analysis the data were binned in 1 second time intervals representing a pixel size of 300 m x 3 km. The detector operates at 1064 ± 1 nm and measures the reflected signal strength to about 1%, and the receiver performance closely matches pre-launch testing. For the seasonal variations of interest in the present analysis the stability of the measurement is more important than the absolute calibration.

In this passive mode the radiometry is only obtainable when the surface of Mars is illuminated by sunlight. Further, since the orbit of the spacecraft is approximately sun-synchronous with a 2:00 PM local time the data are generally acquired under similar lighting conditions.

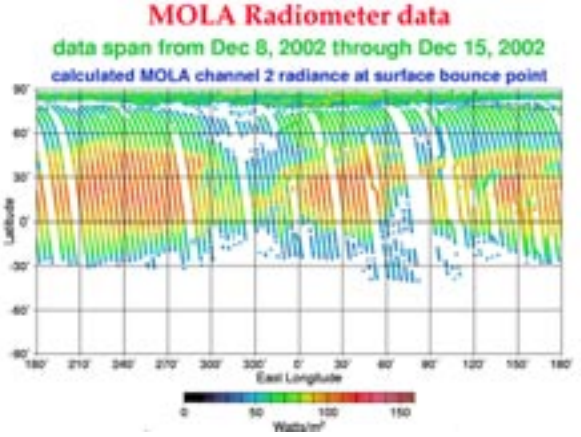

Fig. 1. *Uncalibrated passive radiometry observations acquired by MOLA between Dec 8 and 15, 2002. During the observation period the season was northern summer, with the sun illuminating the northern hemisphere of the planet. An example of the spacecraft being pointed off-nadir is evident in the figure at lat 25° N, 55° E. The spacecraft was traveling from south to north.*

However, the spacecraft instrument deck is not always pointed toward nadir and for much of the last year has been tilted off-nadir

by approximately 16^o in order to save on propellant used for attitude control. Further, the spacecraft is frequently rolled and pitched toward a particular target for camera observations, and the MOLA detector field of view follows the same path (Fig.1).

Seasonal Changes. The radiometry data show clear seasonal brightness changes in the polar regions that are a result of the deposition and sublimation of CO_2 on the surface at the onset of fall and in early spring. Fig. 2 shows the reflectivity at 1064 nm at the beginning of spring and early summer in the 2 hemispheres. Generally, the frost deposition in the north is distributed uniformly in longitude except on the polar cap itself, where the deposition and the sublimation appear to be related to the topography of the cap. In general areas that are less bright are lower in elevation and receive less solar illumination.

In the south the frost covering varies significantly with latitude and longitude (Fig. 2) and some regions appear even in early spring to have lost all their seasonal covering of CO_2. In contrast to the north polar region, the brightest regions do not correspond to those of highest elevation. The residual cap remains bright throughout the year and is probably a result of the exposure of water ice under the seasonal frost.

Seasonal frost on the southern polar residual cap is brighter than in the north and lasts longer in the spring. Both seasonal caps brighten as winter proceeds, and the brightness of both caps oscillates just before the frost sublimates back to the atmosphere, most markedly in the north. This phenomenon is observed in consecutive Martian years.

Observations of the process of frost deposition are more difficult to obtain due to most of the frost at high latitudes being deposited when the region is in darkness. However, the radiometry data do suggest that frost at the higher latitudes actually starts to form on the surface before the end of summer when the sun is approaching the equator but the pole is still illuminated. For the high northern latitudes this appears to begin around L_s= 150^o. The frost covering at both poles appears to have been similar, but not identical, in the two successive Mars years so far studied.

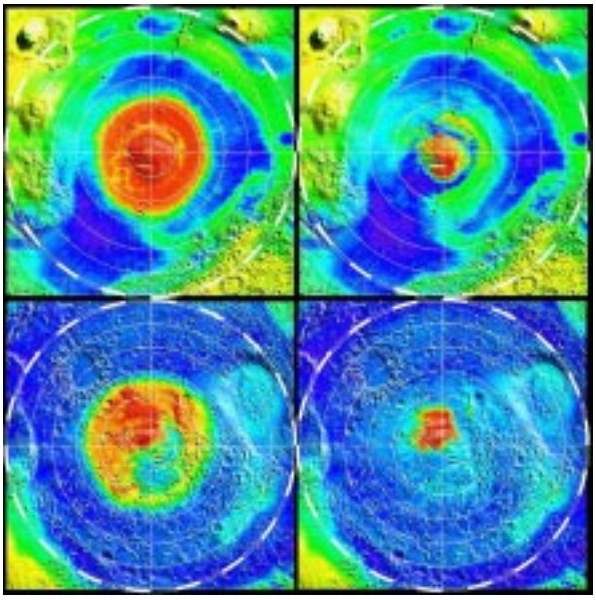

Fig. 2. *Seasonal images of the 1064-nm reflectance in the polar regions in early spring and early summer. The top 2 images are of the northern hemisphere (30^{o}N to pole) for L_s= 32^o (left) and L_s= 12^o (right). Bottom 2 images are of the southern hemisphere (30^o S to pole) for L_s= 212^o (left) and L_s= 272^o (right).*

References. [1] Zuber M.T. et al. (1992) *JGR, 97,* 7781-7797. [2] Smith D.E. et al. (2001) *JGR, 106,* 23,689-13,722. [3] Abshire J.B. et al. (2000) *Appl. Opt., 39, 90,* 2440-2460. [4] Albee A. et al. (2001) *JGR, 106,* 23,291-23,316. [5] Sun, X., et al. (1992) *IEEE Trans. Aero. Elec. Syst.,28,* 268-274. [6] Sun X. et al., (2001) *EOS Trans. Am. Geophys. Un.* [7] Gardner C.S. (1992) *IEEE Trans. on Geosci. Rem. Sens., 30,* 1061-1072.

SEASONAL ADVANCE AND RETREAT OF MARS' SOUTH POLAR CAP AS MEASURED BY THE MARS ODYSSEY NEUTRON SPECTROMETER. T. H. Prettyman,[1] W. C. Feldman,[1] J. R. Murphy,[2] H. O. Funsten,[1] D. J. Lawrence,[1] R. R. Linn,[1] S. Maurice,[3] and R. L. Tokar,[1] [1]Los Alamos National Laboratory, Los Alamos, New Mexico, [2]New Mexico State University, Las Cruces, New Mexico, [3]Observatoire Midi-Pyrenees, Toulouse, France.

Introduction: The Martian seasonal polar caps consist of CO_2 frost deposits that advance towards lower latitudes during fall and winter and retreat toward the poles during spring and early summer in response to seasonal changes in insolation [1]. Because a large portion of the atmosphere is cycled in and out of the seasonal caps during the year, the frost deposits play a significant role in regional and global atmospheric circulation. Surface thermal properties as well as local atmospheric temperature and pressure influence the onset of frost deposition. The presence of dust in the atmosphere affects the polar energy balance, and can influence the rate of deposition and sublimation of frost [2]. During southern summer, the south polar cap is covered by residual CO_2 frost [3].

In this study, we determine the spatial distribution, areal density, and total inventory of the seasonal CO_2 frost in the southern hemisphere using neutron spectroscopy. In contrast to telescope observations and orbital photography, neutrons provide a direct measurement of the areal density (with units of g/cm^2) of CO_2 surface ice, which we refer to as "thickness" in this abstract. However, the surface spatial resolution that can be achieved by neutron spectroscopy is coarse, on the order of 600 km full-width-at-half-maximum. Nonetheless, the regional-scale resolution of neutron spectroscopy is sufficient for validation of circulation models and for comparison with previous observations.

Results reported in this abstract were obtained using data acquired by the neutron spectrometer subsystem of the Mars Odyssey gamma ray spectrometer while in mapping orbit during the years 2002 and 2003, from L_S=330° through L_S=180°. This period of time includes the advance of the seasonal frost in the south. By mid-September (L_S=260°), the frost will have fully retreated, exposing the residual terrain. Consequently, we will report details of the advance and retreat of the frost at the conference.

Advance of the seasonal frost: A map of thermal neutron count rates in the high southern latitudes obtained during southern summer (330°<L_S<0°) is shown in Fig. 1. Thermal neutrons are the portion of the population of neutrons produced by cosmic ray interactions with Mars that achieve thermal equilibrium with the surface. The relatively low count rates poleward of -55° observed during summer correspond to a terrain rich in water-equivalent hydrogen that was recently discovered by Mars Odyssey [4,5].

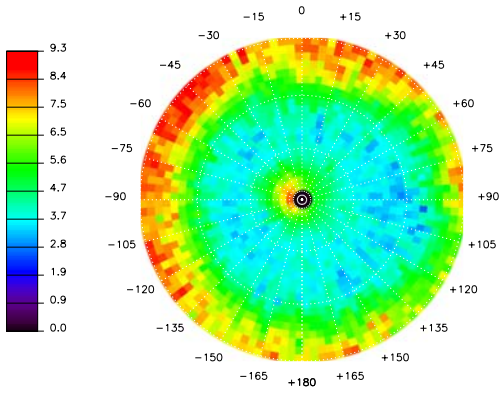

Fig. 1. Map of thermal neutron count rates in the southern high latitudes (poleward of -45°) during late summer. The units are counts per second.

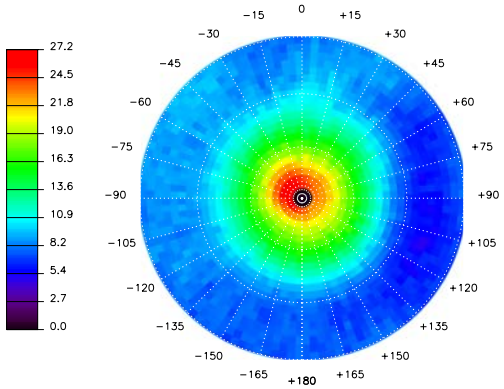

Fig. 2. Map of thermal neutron count rates in the southern high latitudes (poleward of -45°) during late winter. The units are counts per second.

The population of neutrons in thermal equilibrium with the surface is very sensitive to the presence of CO_2 frost, which is an excellent neutron moderator that is also a poor thermal neutron absorber. Consequently, the seasonal deposition of frost causes the output of thermal neutrons to increase. For this reason, the south polar residual cap, which is covered by CO_2 ice, is associated with enhanced thermal neutron count rates relative to the surrounding water-rich terrain, which can be seen in Fig. 1 [6]. The residual cap is centered at about -50° east longitude and is offset approximately 3° from the pole.

As the southern winter progresses, CO_2 frost deposits form and advance equatorward. Fig. 2 shows

the thermal neutron map late in the southern winter ($140°<L_S<180°$) as the frost is approaching its maximum coverage. Note that the region of enhanced count rate has expanded around the residual cap to produce an irregular boundary that extends equatorward beyond -60°. The maximum count rate, which corresponds to maximum frost thickness, is roughly centered on the location of the residual cap.

Thickness of the seasonal frost: We developed an algorithm to determine the distribution and thickness of the seasonal CO_2 frost from thermal neutron count rates. The neutron output observed during summer was used to minimize the sensitivity of the thickness determination to variations in the composition of the underlying terrain. The effect of possible enrichment of N_2 and Ar, which are strong thermal neutron absorbers, in the polar atmosphere during winter was ignored in the present analysis [7]. Consequently, lower bounds on frost thickness are presented.

The time-evolution of CO_2 frost thickness determined from longitudinally-averaged thermal neutron count rates is shown in Fig. 3. The time interval for each measurement was 5° of L_S. The measurements can be compared to frost thicknesses calculated by the Ames Research Center General Circulation Model (ARC-GCM). The ARC-GCM is a comprehensive model of the Martian atmosphere that treats the seasonal condensation and sublimation of CO_2 frost to and from the surface, taking into account the dynamics of the atmosphere, surface thermal properties and the effect of atmospheric dust on the rate of frost deposition and sublimation [8.9]. Calculated frost thicknesses are shown in Fig. 4 for latitudes that fall within four of the zones defined in Fig. 3. When comparing Figs. 3 and 4, note that the L_S scales are different.

Predictions of frost thickness by the ARC-GCM are similar in magnitude and shape to the measured values. The measurements indicate that frost forms later and achieves maximum thickness earlier at lower latitudes than near the poles, which is predicted by the model. The measured times of peak frost thickness, however, are slightly later than predicted and the frost recession is not as rapid as modeled. The relatively slow frost recession may be caused by increased atmospheric dust compared to the model. The measured inventory of CO_2 frost in the southern seasonal cap achieves a maximum value of 8×10^{18} g between 160° and 170° L_S, which is slightly more than 30% of the established value for total atmospheric mass (2.5×10^{19} g).

This comparison demonstrates the utility of thermal neutron count rates for determining absolute frost thickness with high temporal resolution. Further work is being carried out to improve the spatial resolution of the measurements using forward models of the instrument response, and spatial deconvolution techniques. Corrections for atmospheric composition will also be implemented. A comparison of our measurements to the ARC-GCM and observations of the seasonal frost in previous years will be presented.

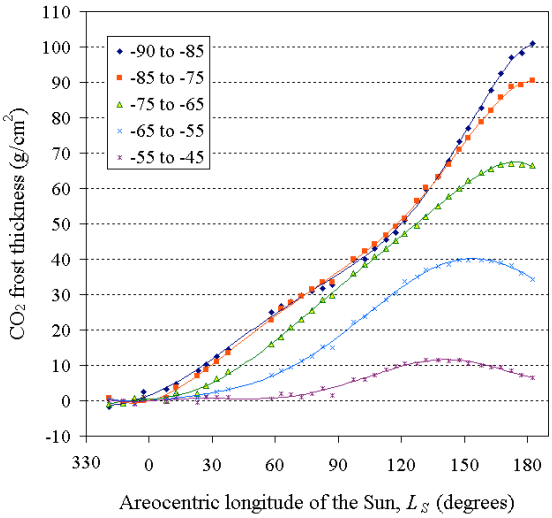

Fig. 3. Seasonal CO_2 frost thickness determined from longitudinally-averaged thermal neutron count. Latitude ranges for each zone are shown in the legend.

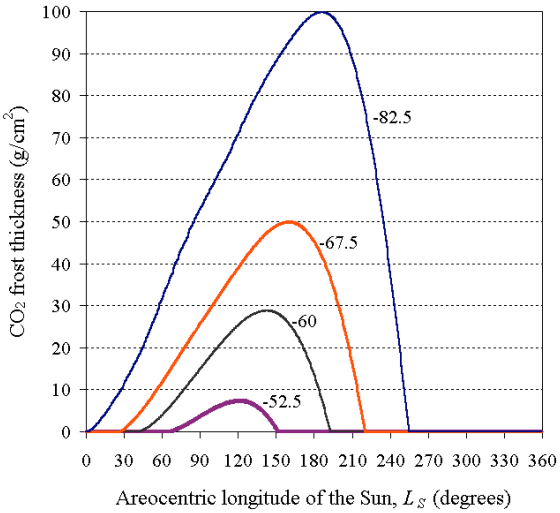

Fig. 4. Seasonal frost thickness in the southern latitudes predicted by the ARC-GCM for four latitudes (-82.5°, -67.5°, -60°, and -52.5°).

References: [1] Neugebauer, G., et al., *Astron. J.* 76, 719-749, 1971. [2] James, P. B., et al., *JGR* 84 (B6), 2889-2922, 1979. [3] Kieffer, H. H., *JGR* 84 (#SI), 8263-8288, 1979. [4] Boynton, W. V., *Science* 297 (#5578), 81-85, 2002. [5] Feldman, W. C., *Science* 297 (#5578), 75-78, 2002. [6] Tokar, R. L., et al., *GRL* 30 (#13), 1677, doi:10.1029/2003GL017316, 2003. [7] Feldman, W. C., et al., JGR in press, 2003. [8] Pollack, J. B., et al., *JGR* 95 (#B2), 1447-1473, 1990. [9] Haberle, R. M., *JGR* 104 (#E4), 8957-8974, 1999.

CONSTRAINTS ON THE WITHIN SEASON AND BETWEEN YEAR VARIABILITY OF THE NORTH RESIDUAL CAP FROM MGS-TES. W.M. Calvin[1], T.N. Titus[2], and S.A. Mahoney[1]. [1]Dept. of Geological Sciences, MS172, University of Nevada, Reno, NV 89557, wcalvin@unr.edu, [2]U.S. Geological Survey, Flagstaff, AZ 86001, ttitus@usgs.gov.

INTRODUCTION: There is a long history of telescopic and spacecraft observations of the polar regions of Mars. The finely laminated ice deposits and surrounding layered terrains are commonly thought to contain a record of past climate conditions and change. Understanding the basic nature of the deposits and their mineral and ice constituents is a continued focus of current and future orbited missions. Unresolved issues in Martian polar science include a) the unusual nature of the CO_2 ice deposits ("Swiss Cheese", "slab ice" etc.) b) the relationship of the ice deposits to underlying layered units (which differs from the north to the south), c) understanding the seasonal variations and their connections to the finely laminated units observed in high-resolution images and d) the relationship of dark materials in the wind-swept lanes and reentrant valleys to the surrounding dark dune and surface materials.

Our work focuses on understanding these issues in relationship to the north residual ice cap. Recent work using Mars Global Surveyor (MGS) data sets have described evolution of the seasonal CO_2 frost deposits [1-5]. In addition, the north polar residual ice cap exhibits albedo variations between Mars years and within the summer season [4-6]. The Thermal Emission Spectrometer (TES) data set can augment these observations providing additional constraints such as temperature evolution and spectral properties associated with ice and rocky materials. Exploration of these properties is the subject of our current study.

MGS-TES DATA SET: Mars Global Surveyor began systematic mapping of the planet in March of 1999. The Mars season was early northern summer, L_s=104. As Kieffer and Titus [2] noted, the seasonal CO_2 frost had disappeared by that time and they observed the growth of higher albedo regions (onset of winter frosting) beginning at $L_s \sim 164$. James and Cantor [4] monitored the seasonal cap recession of 2000 and found the signature of the residual cap emerging under the seasonal CO_2 frost between L_s 60 and 70. We somewhat arbitrarily mark our timeframe of interest as L_s 65 to 165. This allows study of the albedo, temperature and spectral properties of the residual cap through the seasonal cap and the "bare" residual cap. In this regard we can compare variations within the summer season to properties observed under thin or sparse CO_2 frost coverage. The table below illustrates that there are two full and one partial northern summer seasons of data acquired. The data from the first two summers are available via the PDS and the second full summer's data are being released over the next several months.

Northern Summer	L_s 65	L_s 165	Mission Phase
1-partial	4-Dec-98 (pre-mapping)	5-Jul-99	Map
2-full	20-Oct-00	22-May-01	Map/Ext
3-full	8-Sept-02	9-Apr-03	Ext-Ext

PREVIOUS OBSERVATIONS: Earlier workers noted the change in albedo in a number of north pole bright outliers and in the overall coverage by bright ice deposits both between Viking summers and between Viking and Mariner 9 [6-8]. This was possibly attributed to the affects of global dust storms [8]; however Bass et al. [6] showed that significant within season variation occurred among Viking imagery. Cantor et al. [5] also explored this variation in MOC images and noted brightening at the edges within a given Mars summer season and changes in the cap appearance at the same L_s between MGS years (1 and 2 as defined in the table above). The early season appearance was possibly attributed to the occurrence of a large dust storm the previous year, and it was noted that late season ice extent recovers to Viking levels but exhibits small-scale inter-year variations that may not be related to globally repeated weather events [5].

These brightness variations are most extensively observed in the quadrant from 0 to 120 east longitude (lower right) on a polar stereographic projection (see Figures 1 and 2). Typically the large "tail" below the Chasma Boreal and its associated plateau (see Zuber et al. [9] for topography) remain bright while highly sloped cap edges and valleys are defrosted in the early season. Malin and Edgett [10, Figure 76] also call out variations on the end of the southern "tail" (-15 to -40 longitude) and in spiral structures above the Chasma Boreal observed at the same L_s in different Mars years. We note there also appears to be substantial frost variation at the "source" of Chasma Boreal (10 to 25E) from Viking to recent years, being darker in the present epoch in MOC and TES albedos than it was during Viking (Figures 1 and 2).

PRELIMINARY RESULTS: We are examining these seasonal and interannual variations of the north cap in the TES data set. This includes comparison of TES albedo with visible appearance in MOC imagery, merging TES, MOC and Viking data with high-resolution topography, and mapping spectral properties associated with seasonally varying and more constant units within the north residual cap. Figure 2 shows initial results for the early season of MGS "Summer 2" acquired from 12/20/00 to 1/03/01 or L_s ~ 92 to 98. Early season "defrosted" units are seen quite similar to the MOC and Viking results [5, 6, and 10] described in the preceding section. We will present the evolution of TES albedos within this MGS northern summer and the ability to use temperature and slope as a proxy for units which are susceptible to summer and annual changes.

TES spectra are notoriously difficult to work with for these cold polar temperatures. Kieffer et al. [1] show representative examples, but typically use large regional averages to improve the signal-to-noise, especially at higher wavenumbers (>1200 cm-1) where the radiance is dropping rapidly. In an effort to examine seasonal trends they developed several multichannel "bands" and used brightness temperatures (T_b) of these broadband averages and their differences to define surface units. Kieffer and Titus [2] presented data either longitudinally averaged or using these broadband temperatures. We are currently developing methods of handling the spectral variations including use of 2-temperature models to fit mixed pixels of warm rock and cold ice as well as cold surfaces under a warmer atmosphere (e.g. [11]). We will report on the status of various methods and their comparison to previous approaches. We will present preliminary spectral characteristics of ice units that are seasonally variable, seasonally stable and of non-ice units both within and surrounding the residual north cap.

REFERENCES: [1]Kieffer et al, *JGR*, **105**(E4), 9653-9699, 2000. [2]Kieffer and Titus, *Icarus*, **154**, 162-180, 2001. [3]Titus et al. *JGR*, **106**(E10), 23181-23196, 2001. [4]James and Cantor, *Icarus*, **154**, 131-144, 2001. [5]Cantor et al. *JGR*, **107**(E3), 10.1029/2001JE001588, 2002. [6] Bass et al. *Icarus*, **144**, 382-396, 2000. [7] Kieffer, *JGR*, **96**, 1481-1493, 1990, [8] Paige et al. *JGR*, **99**, 25959-25991,1994. [9] Zuber et al. *Science*, **282**, 2053-2060, 1998. [10] Malin and Edgett, *JGR*, **106**(E10), 23429-23570, 2001. [11] Hanel et al., *Exploration of the Solar System by Infrared Remote Sensing*, 1992.

ACKNOWLEDGMENTS: This material is based on work currently supported by NASA under the MDAP Program, Grant: NAG5-12223 to the University of Nevada, Reno and through the 2005 Mars Reconnaissance Orbiter MARCI/CTX Science Team. Viking base image of Mare Boreum courtesy of NASA and obtained through the Planetary Photojournal Web Site at the USGS Flagstaff.

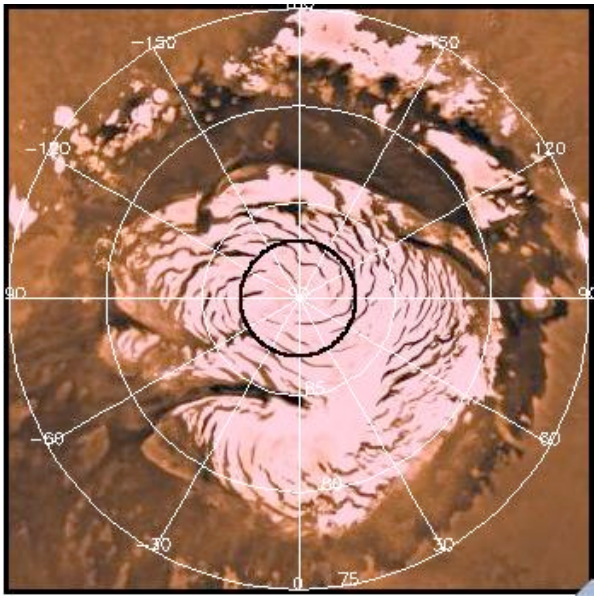

Figure 1: North residual cap as observed by Viking. Black ring denotes area within which TES does not acquire data.

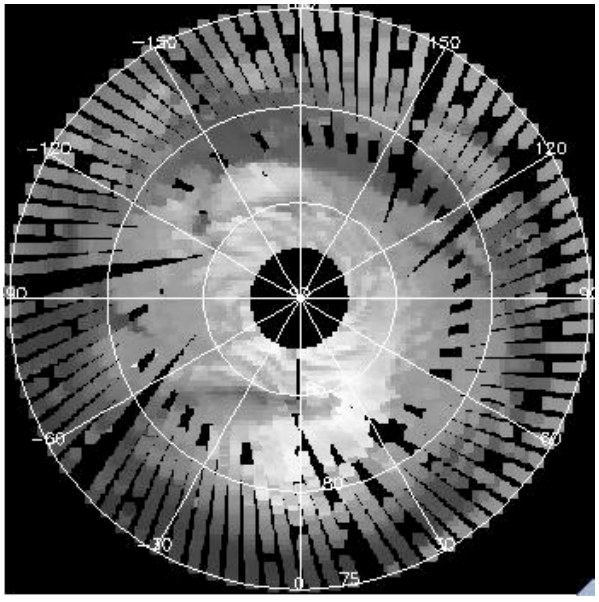

Figure 2: TES albedo map Ls~95 (Dec00/Jan01). Note the lack of bright areas from 30 to 120 E longitude, the extent of Chasma Boreal and the shape of ice surfaces below the Chasma compared with Viking. Squares do not model TES pixel size.

SOUTH POLAR CRYPTIC REGION REVISTED: THEMIS OBSERVATIONS. T. N. Titus[1], H. H. Kieffer[1], J. J. Plaut[2], P. R. Christensen[3], A. B. Ivanov[2], and the THEMIS Science Team[3], [1]USGS, 2255 N. Gemini Dr., Flagstaff, AZ 86001; email: ttitus@usgs.gov, [2] JPL, Pasadena, CA, [3] ASU, Tempe, AZ.

Introduction: The early part of the Mars Global Surveyor mission provided good TES coverage of the Mars south polar region. These data allow mapping of the polar cap recession, surface and atmospheric temperatures, and albedo features found within the seasonal cap itself [1,2] over L_s = 180° – 270°. During this period, the seasonal south polar cap retreated continuously and asymmetrically around the geographic pole, similar to the observations of Viking in 1976-1977 [3]. A prominent albedo feature on the seasonal cap is a region that appears almost as dark as bare ground, yet remains cold. (See Figure 1.) We refer to this region, generally located between latitudes 85°S and 75°S and longitudes 150°W and 310°W, as the Cryptic region.

Past Observations: A re-examination of the IRTM data revealed that the Cryptic Region was not unique to the TES era, but also was apparent during the Viking IRTM era. (See Figure 2.) Interestingly, Antoniadi [4] observed dark regions forming on the seasonal cap that loosely correlate to the Cryptic region: Depressio Magna (1909) and Depressio Parva (1929). These *depressios* were located at 270° W, 78°S and 166° W, 76°S, respectively.

Analysis of both the TES and IRTM data indicate that the Cryptic region is unique in its thermophysical properties relative to the rest of the cap. The region occupies the same general area from year to year. It is darker and slightly warmer than the rest of the south polar cap. Even though the Cryptic region is slightly warmer, it must still be CO_2-buffered since it remains "cold" for several days.

Spectral analysis of the TES data longward of the 15-micron atmospheric band shows that the Cryptic Region shows less spectral contrast than the rest of the polar cap. This suggests that the region may be composed of "ice," as opposed to snow or frost [5].

The Vent Hypothesis: Since the initial discovery of the Cryptic Region, several surface features, referred to as spiders, fans, and Dalmatian spots on the basis of their appearance, have been seen. The fans and spiders correlate to the location of the Cryptic Region [6]. Kieffer [7,8] suggested that the spiders, fans, and Dalmatian spots are the result of CO_2 vents, caused by basal heating of CO_2 deposits. This can only be possible if the CO_2 is at least partially transparent to visible solar radiation and opaque to thermal IR, thus creating a solid greenhouse effect. The CO_2 would sublimate from the bottom of the ice slab, thus building up pressure until the gas can be released through a vent. The gas would transport dust from underneath the ice, through the vent, resulting in dust plumes. This hypothesis is consistent with past observations.

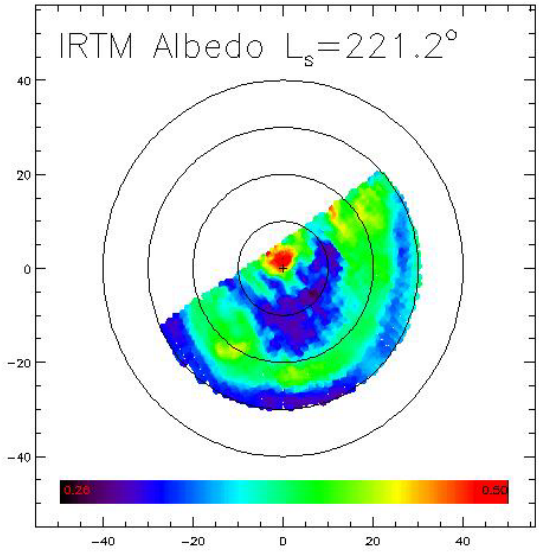

Figure 1: Viking IRTM Albedo Mosaic. This is a mosaic of IRTM visible data taken at L_s = 221.2°. The dark blue feature near the center of the image is the Cryptic region. The latitude lines are drawn at 10° intervals and 0° longitude is up. The region poleward of 65°S is at CO_2 temperatures.

THEMIS Results: THEMIS has the advantage over previous observations in being capable of taking VIS and IR images simultaneously at 18-meter and 100-meter resolution, respectively. Early in the spring, THEMIS observations of Dalmatian spots showed no thermal structure that differentiated the dark albedo areas from the rest of the surrounding seasonal cap. However, by L_s = 206°, thermal structure could be seen. (See Figure 2.) The warmer areas have an increase in brightness temperature of only 5 K over thermally bland areas that are covered by seasonal CO_2 deposits, which is consistent with TES observations at the 3 km scale [9]. These warm areas loosely correlate to the darker albedo areas, as seen in Figures 2 and 3. The spectra of a thermally bland area and an area interior to the three-legged "starfish" show an increase in brightness temperature over the spectral range of 9 μm to 12.5-μm. There are two possible causes for the increase in brightness temperature between these two areas: either the "starfish" surface is warmer than

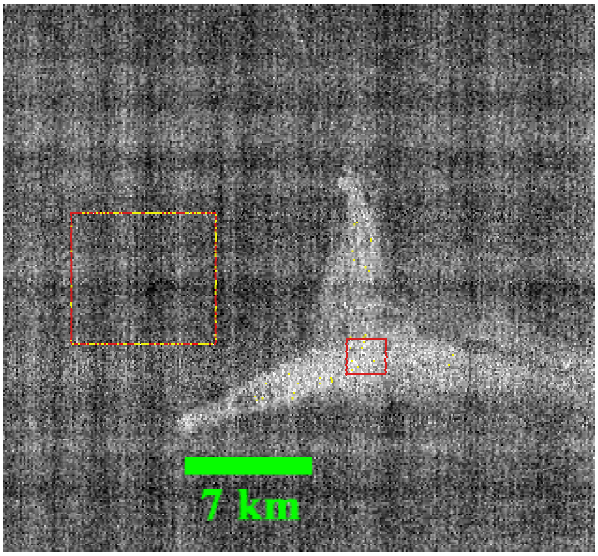

Figure 2: THEMIS IR Image I06707008 (Band 9). This THEMIS IR image shows thermal structure on the seasonal CO2 cap. Spectra were extracted from two locations, the center of the "starfish" and a thermally bland region, representative of seasonal CO_2.

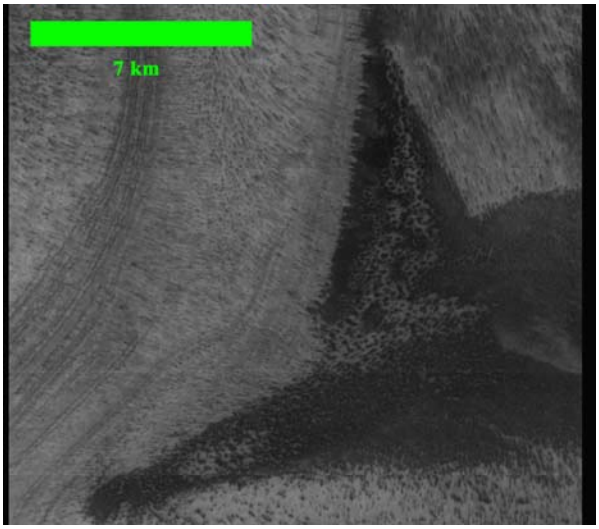

Figure 3: A THEMIS VIS Image V06707009. This THEMIS VIS image shows the same location as the IR image in Figure 2. Notice that the dark albedo region only loosely correlated to the thermal structure seen in Figure 2.

the surrounding area or the local atmospheric opacity is greater than the surrounding atmosphere. If the increase in brightness temperature is due to an increase in the kinetic temperature of the surface, then the spectra have an absorption feature at 11-12 µm. However, if the increase in brightness temperature is due to in increase of atmospheric opacity, perhaps from a nearby dust plume, then the spectra have emission features at 9-10 µm and 12.5 µm. The 9-10 µm spectral region is where atmospheric dust has a peak in opacity. The 12.5-µm region is where water ice clouds have a peak in opacity. The combination of these two spectral peaks in brightness temperature is suggestive of water ice-coated dust grains. Atmospheric emission features are a more plausible explanation of the THEMIS spectra than is an absorption feature at 11-12 µm. The atmospheric opacity explanation of the THEMIS spectra is consistent with the geyser hypothesis.

Summary: We will present the most current THEMIS observations of the Cryptic region. These data, combined with TES data and MOC imaging, will be used to test the Kieffer geyser model.

References: [1] Kieffer, et al. (1998) In LPSC XXIX, Abstract #1481. [2] Titus, T., et al. (1998), BAAS, vol. 30, no. 3, 1049-1050. [3] Kieffer, H.H. (1977) JGR, 82, 4249-4291. [4] Blunck, J (1977) "Mars and its Satellites: A detailed Commentary on the Nomenclature". [5] Hansen,G. (1998) JGR, 104 , 16,471. [6] Piqeux, S. (2003) JGR, Submitted. [7] Kieffer, H. H. (2001) Second International Conf. On Mars Polar Sci. and Exploration, #1057. [8] Kieffer, H. H. (2003), Sixth International Conference on Mars, #3158. [9] Kieffer, H. H. et al. (2000) JGR, 105, 9653.

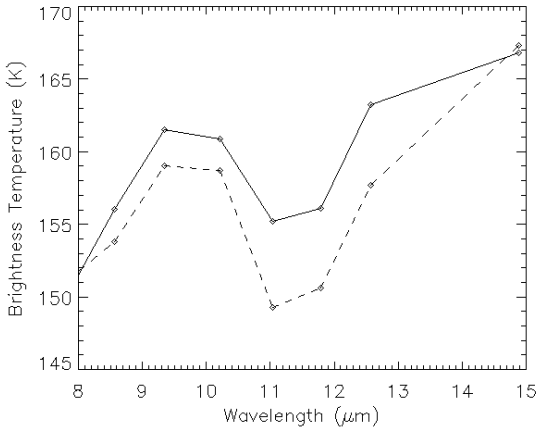

Figure 4: THEMIS IR Spectra. This is a plot of two spectra extracted from THEMIS image I06707008. The solid line is the spectrum extracted from the area inside the small red box (Figure 2). The dashed line is the spectrum extracted from the area in the larger red-yellow box (Figure 2). The 15 µm brightness temperature is an atmospheric temperature.

BEHAVIOR OF SOLID CO_2 ON MARS: STILL A ZOO. Hugh H. Kieffer, *U. S. Geological Survey [Emeritus], Flagstaff, AZ 86001, USA, (hkieffer@uneedspeed.net).*

Observations of the martian polar caps by TES, THEMIS and MOC have revealed a variety of peculiar patterns: now informally known as **Cryptic material, Dalmatian spots, spiders, oriented fans and fried eggs**. These result from the characteristics and behavior of solid CO_2 on Mars, which is unlike anything on Earth. The proposed model involves the micro-physical interaction of CO_2 and dust with the solar and thermal radiation fields on Mars. This abstract is a shortened version of that for Mars VI, with no citations.

CO_2 Surface Condensation Modes: The condensation of the predominant gas in an atmosphere by radiative cooling yields the prominent seasonal polar caps on Mars. This process has no terrestrial analogy, which limits our intuition. This process is difficult to impossible to simulate in the laboratory because the natural force that allows condensation at a location other than at the coldest boundary (which sets the radiation balance) is gravitation, involving a characteristic scale many km. A practical laboratory scale would require a warm physical barrier that is completely transparent to thermal radiation.

TES observations in many areas in the polar night indicate that most of the condensation occurs at the Martian surface. TES spectra in the 25 μm region indicate that the "**Cryptic**" regions of cold-dark polar material consist of a CO_2 non-scattering slab composed of indeterminately large grains, or a slab. In other regions, fine-grained frost is found.

For condensation of a nearly pure gas by radiative loss there can be two end-member solutions for the form of the solid. If the abundance of non-condensing gases is negligible, so that a diffusion gradient of the condensing material is not involved, then a thick slab can form. On Mars, the dominant radiative loss of the condensate is from inside the bulk material. Growth perturbations outward from a planar solid interface, such as a crystal spike growing upward, have a longer conductive path to the bulk solid which, in turn, can radiate the latent heat of condensation. Lacking a diffusion gradient at the tip of such a spike, the condensation rate is limited by conductive heat loss, and this tip is at a disadvantage for condensation relative to the bulk solid. Thus perturbations do not grow, and the expected steady state form is a thick slab with a smooth surface. Such slabs are observed to grow in laboratory conditions of pure condensing gases, althoughthe thermal gradient internal to the slab results from conduction to a cold substrate rather than by radiative cooling.

In the presence of some amount of non-condensing gas, e.g., the 5% of N_2 plus Ar on Mars, at the micro-physical level there will be some diffusion gradient of the condensing gas toward the condensation sites. Both the temperature gradient and the concentration gradient of the condensate are expected to be linear for steady state conditions. Because of the nonlinear dependence of saturation pressure upon temperature, the partial pressure will be above the saturation pressure throughout this layer. Under this condition,spikes sticking up into this diffusion gradient become the favored site of condensation and they will grow more rapidly than locations deeper into the diffusion gradient. The steady state solution for the form of such a growing deposit is long columnar crystals oriented along the diffusion gradient. Such deposits also are observed to form in laboratory conditions of substrate cooling when small amounts of non-condensing gas are introduced into the chamber . This process of growth in a diffusion gradient gives rise to the beautiful H_2O hoar-frost crystals seen on calm terrestrial winter mornings.

TES observations indicate that both the slab growth and deposition of fine-grain CO_2 condensates occur in the polar night and that different condensation processes are dominant in different locations. The reason for the geographic distribution of the Cryptic material is unknown.

Radiation Balance in a Pure Solid CO_2 Slab: During the polar night, the radiative balance of surface CO_2 will be negative (barring an extraordinarily warm atmosphere). With the Sun above the horizon, solar radiation penetrates deeply into pure CO_2 . The relative absorption lengths for solar and thermal energy become important.

Using the optical properties of solid carbon dioxide, the penetration of both solar energy and ambient thermal radiation into a slab of CO_2 have been calculated. For typical polar summer conditions (incidence angle of 65°, $U = 1.5$), 2/3 of the solar energy penetrates 1m into pure solid CO_2 , whereas thermal flux is reduced to 50% in 3.7 mm. The top 2 mm of the slab are in net radiative loss; below that absorption of insolation results in net heating.

Dirty CO_2 Ice: Mars atmosphere is generally dusty with particles of radius on the order of 2 μm. During the CO_2 condensation season, atmospheric dust grains probably act as condensation nuclei; perhaps first for H_2O and then for CO_2. The proportion of dust in the CO_2 cap has not been measured, but is reasonably assumed to be near the average abundance of dust in the atmosphere. Using an average visual opacity of the atmosphere of 0.5 yields a dust abundance of about 1.5×10^{-3} kg m^{-3} or roughly 2×10^{-5} by mass. Because the particle size is smaller than thermal wavelengths, the presence of embedded dust will make little change to the thermal radiation environment, but will shorten substantially the solar absorption lengths, narrowing or removing entirely the surficial layer with net radiation loss.

Using the above values, and densities of dust grains and solid CO_2 of 2300 and 1600 kg m^{-3}, respectively, corresponds to a mean dust grain separation of $\sim$130 μm. If a seasonal cap budget of 1000 kg m^{-2} is adopted, the mass of dust in the cap is 0.02 kg m^{-2} and the geometric opacity of the dust in the cap is $\sim$1.6. The visual opacity of dust in the slab at sunrise will be roughly the average opacity of the southern atmosphere during the condensation season times the ratio of slab to atmospheric mass, or $\sim$3.3, in agreement with the geometric opacity if the scattering efficiency is taken as 2.0, as expected from Mie theory.

CO_2 Self Cleaning by Entrained Dust Movement: A first approximation is that for a dirty CO_2 slab, all of the solar energy is absorbed by the dust grains. However, because the surrounding CO_2 is isothermal, this radiation absorbed

by the grains must go into sublimation of solid CO_2 . If the local material is impermeable, a high-pressure pocket of gas will form around the grain and local elastic deformation will increase the pressure in the solid CO_2 , allowing some heat to be absorbed without sublimation. The warmer grain cannot be in direct contact with the CO_2 , but must rest on a microscopic layer of gas at the bottom of its vapor prison. If the local gas bubble does not rupture, there will be a downward migration of the bubble through the solid as vapor re-condenses on the roof of the bubble, the location most distant from the grain and hence coolest, and the grain will "burrow" downward as sublimation continues under the grain. Thus, a sealed finite vertical columnar hole will travel downward with the grain. When the grain reaches the bottom of the impermeable layer, it will be ejected downward. This self-cleaning, self-annealing process will tend to reduce the amount of dust in the ice through the spring. Because the net solar flux is greater toward the top of the slab, the uppermost particles will move most rapidly, resulting in concentration of dust as a descending "curtain" in the slab, leaving clean ice above.

Development of Pathways and Vents: The net positive radiation divergence near the surface of pure CO_2 will tend to seal small holes in the surface layer. Porosity will generally be sealed in a region that grows downward from the surface. Thus, the gas formed by springtime sublimation generally cannot diffuse upward through the CO_2 deposit. The gas resulting from net sublimation below the surface must escape somewhere and will hold open some set of larger holes. Because the gases in these vents will have some entrained dust, they can continue to absorb solar radiation, transfer energy to the vent walls, and remain open and grow. Also, gas under an impermeable CO_2 slab could reach pressures several times the atmospheric surface pressure. The saturation temperature under a 1000 kg m^{-2} slab would be 162K, enhancing the ability of venting gas to enlarge the pathways. Because higher velocities are possible and because of the r^2 heat flow versus the r^1 circumference, larger holes/paths will grow at the expense of smaller ones. Gas released beneath the slab must find some path to the open atmosphere. It may travel laterally underneath the slab to vents, cracks, or even to the edge of the seasonal deposit. It is difficult to predict the spacing of such vents, but they collectively must carry the total sublimation gas flux of about 10 kg m^{-2} /day. Vent spacing of tens to hundred meters is observed.

As the effective vents are separated by substantially more than the slab thickness, gas velocities will become far greater than required to suspend dust particles, and any sub-slab lateral transport may begin erosion of underlying loose material. Once the velocity exceeds the fluid threshold, erosion will begin.

The sub-slab lateral gas velocity will depend upon the geometry of the flow; increasing toward a vent. Because the soil thermal inertia of the Cryptic region is low, it is likely that the surface material is incohesive and that channelized flow will develop by scouring, beginning near the vents and progressing outward. Although velocities on the order of 10 m/s are required to initiate transport of fine material by saltation, injection of dust released from the CO_2 into the lateral flow may initiate motion and scouring at lower velocities; 2 mm/s vertical velocity is adequate to maintain atmospheric dust in suspension.

Dark radially converging dendritic patterns are visible in MOC images of some portions of the spring polar cap, these have been termed " **spiders**" by the MOC team. In this model, these patterns represent channels formed by sub-slab channelized flow of the sublimation gas toward the vents. Increasingly large particles could become entrained closer to the vent.

The velocity in the vents will be approximately $.005X^2$ m/s, where X is the ratio of vent separation to vent diameter. For example, for vents 1 m in diameter spaced by 100 m, the gas velocity would be 50 m/s. When the jets exhaust into the atmosphere and velocities decrease, the coarser entrained material will fall out in the prevailing downwind direction. In this model, the oriented dark **fans** seen in the MOC images are caused by this process. This is an exotic model that agrees with observations thus far. It predicts that the dark fans will be oriented into the prevailing wind, that they are seasonal and will disappear with, or shortly after, the CO_2 is gone, and that the "spiders" will be found only in the Cryptic region.

Darks vents are generally, but not exclusively, associated with dunes. Vents can progress into dark spots (**Dalmatian spots**) which grow monotonically until they coalesce. Dark halos commonly develop around the Dalmatian spots; these have been termed "**fried-eggs**" based on their symmetry and proportions. Many MOC images of the seasonal cap in summertime show great variegation of reflectance, interpreted to be incomplete solid CO_2 cover . Sequences of images show the development of evenly-distributed circular darks spots, which may represent the evolution of vents, commonly spaced by order 100 m, that gradually expand to consume the seasonal cap.

This model has been supported by a survey of the location of "spiders" in MOC imaging which shows that they are largely confined to the Cryptic region and their centers generally correlate with the location of fans. Spiders commonly persist as low relief features through the summer.

Most of this story has been developed from observations of the south polar cap. The north and south caps seem to be somewhat different in terms of the abundance of these features; e.g., spiders have not yet been identified in the north.

Summary: Deep in the martian polar night, there is some CO_2 snowfall, but most of the solid CO_2 takes the form of a uniform, continuous, non-scattering slab with embedded dust (and H_2O ice) grains. Following seasonal sunrise, in some areas the ice brightens due to fracture or surficial frosting, but in other areas the slab persists to form the *Cryptic* regions. The solar energy is largely absorbed by the dust grains, which either burrow downward or escape upward, cleaning the CO_2 slab which anneals small holes near its surface. Sunlight then penetrates to the bottom of the slab, warming the soil and subliming ice from the bottom. Widely spaced vents develop that allow the gas to escape. As the sub-slab gas converges toward the vents, it scours the soil surface along ragged channels (*spiders*). Dust entrained in the jetting gas falls out downwind to form *oriented fans*. The vents enlarge to become *Dalmatian spots*, some of which form *fried-egg* halos; these enlarge to consume the seasonal cap. Only the topographic ghosts of the *spiders* persist through the summer.

EVOLUTION OF LOW-EMISSIVITY SPOTS IN THE MARTIAN WINTER POLAR CAPS: MOBILITY OF DUST GRAINS. G. B. Hansen, Planetary Science Institute, Northwest Division, Department of Earth and Space Science, University of Washington, Seattle, WA 98195 (ghansen@rad.ess.washington.edu).

Introduction: Temporally and spatially variable regions of low 20-μm emissivity occur regularly on the winter polar caps of Mars, as first discovered in Viking orbiter observations [1], and subsequently in spectra returned by the Mars Global Surveyor Thermal Emission Spectrometer (TES) [2, 3, 4]. Although many disparate effects were originally offered to explain these features, the current consensus is that they are caused by regions of relatively fine-grained CO_2 frost, probably the result of snowfall [4, 5], and occurring often in regions of high topographic slopes, implying dynamic atmospheric processes [6]. The dynamic nature of these spots has been demonstrated by repeated TES observations of the same locations [7]. The apparent grain coarsening observed has been explained as a process of "continued condensation" [6] or a sintering process starting from micron-sized grains [7] based on theoretical study by Eluszkiewicz [8]. My mapping of the polar cap composition and properties [9] has suggested another possible process: the movement of dust condensation nuclei from the center of newly fallen snow grains (where they are largely optically hidden) to grain boundaries (where they are fully optically active). This process was suggested by the modeling of low-emissivity spots in which the CO_2 ice grain size is little different from, while the apparent dust content is much smaller than in the surrounding regions.

Observation Details and Calibration: The TES spectra shown here are from revolution 214, in the first science phasing orbit period (SPO-1). It took place in April 1998, with $L_S \approx 304°$, roughly halfway between the winter solstice and the spring equinox. The historical polar cap size is near its maximum extent at this time and extends to 55–60° N. The limit of polar night is at ~69° N, and the spacecraft ground track crosses into sunlight at ~67° N. The data sequence starts on the night side at 59.5° N in western Utopia Planitia (70° W). The maximum latitude reached over the elevated residual polar cap is 86.2° N. The seasonal polar cap extends to ~51.5° N on the day side, in Tempe Terra (257° W).

The TES is a Michelson interferometer measuring from 1650 to 200 cm^{-1} (~6–50 μm) with a spectral resolution of either 6 or 12 cm^{-1}, and a two-channel bolometric radiometer measuring solar (0.3–2.7 μm) and thermal (5.5–100 μm) spectral regions [2, 10]. The finest spatial resolution of TES measurements is <3 km. Observations of the winter polar regions are useful only above 8–10 μm.

There are many artifacts in the polar spectra from the PDS supplied dataset. These were corrected by adjusting instrument sensitivity and darks. The sensitivity is set assuming that it does not change rapidly with time, and that later times in the sequence are better calibrated. The darks measured by pointing the mirror up differ from those when pointed to the side or down [10]. The offset is a very significant fraction of typical polar spectra [3]. The dark level can be estimated by inspecting limb scan sequences. They are adjusted at the short wavelength end from the data, since the radiance from a ~150 K surface is essentially 0 for wavenumbers larger than 1300 cm^{-1}. There is an important high-frequency component to the darks as well, which also appears to vary slightly from revolution to revolution. These patterns are determined by assuming that the surface spectrum averaged over the whole polar cap, outside the atmospheric CO_2 band, is smooth. When these new darks are used, both individual spectra and small averages of spectra are much better behaved, in that the remaining variations have all the characteristics of random noise.

Previous Work: The seasonal polar caps of Mars are composed primarily of solid CO_2, likely mixed with some micron-sized Martian dust and water ice. Many of these dust and water ice grains may be brought in as condensation nuclei for CO_2 snow grains. Each polar cap spectra from this revolution has been analyzed by fitting to model spectra of ternary CO_2-H_2O-dust intimate mixtures, including partial spatial coverage, surface temperatures, and water ice clouds [9]. The dust optical properties are poorly known in the important 20–50 μm region. Those used here are derived from analysis of airborne dust in Mariner 9 infrared spectra [11]. They fit a few low-dust observations, assuming that the surface spectrum is a blackbody. The dust study is continuing by looking at a wider variety of spectra and variable surface emissivity.

The results of this analysis show that the central polar cap is 100% covered by CO_2 deposits, and that the temperature varies as expected (as a function of altitude). The CO_2 grain radius varies between 200 μm and 1 cm, averaging ~1 mm, while the dust mass mixing ratio varies from 100 ppm to 1%, averaging 0.1%, and the water ice mass mixing ratio varies from 0 to 0.1%, averaging ~100 ppm.

There are several low-emissivity regions in the central polar cap, normally indicated by a large brightness temperature difference between 25 and 18 μm. A detail

of the brightness temperature difference, CO_2 grain size, and dust mass mixing ratio over one of these regions as shown in Figure 1. The typical behavior shown here is that the large brightness temperature difference is reflected mostly in the dust mixing ratio, and not the CO_2 grain size, as has been assumed previously [4, 7].

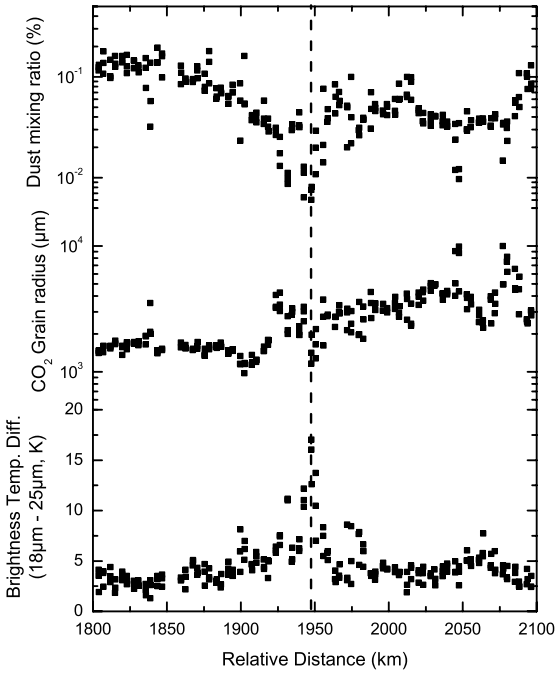

Figure 1

A New Theory: This observation suggests a different process for the temporal and spatial variation of low-emissivity regions. These regions are most likely initiated by fresh CO_2 snowfall from atmospheric dynamic interactions with topographic obstacles. If the CO_2 grains are formed around dust condensation nuclei, the optical properties of the dust are subdued or absent (depending on the ratio of grain size to nucleus size). We will investigate this using layered Mie calculations, but the hiding effect is well known. If the dust nuclei subsequently migrate to the grain boundaries as the deposit matures, the optical effect of the dust will approach the intimate mixing formulation of the models. The effective CO_2 grain size may not change significantly as it matures.

Average spectra from some typical cold spots are shown in Figures 2 and 3. In each case an average from the edges of the low-emissivity region are compared to an average from the center of the region, to show the spectral effect of increased dust at a similar grain size. The background grain sizes is 600 μm, and the dust content varies from 0.01% (center) to 0.1% (edge) in Figure 2, and the background grain size is 2 mm, and the dust content varies from 0.008% (center) to 0.05% (edge) in Figure 3. The background dust mixing ratio is consistent with an original CO_2 grain size of 12–15 μm around a 2-μm dust nucleus.

Figure 2

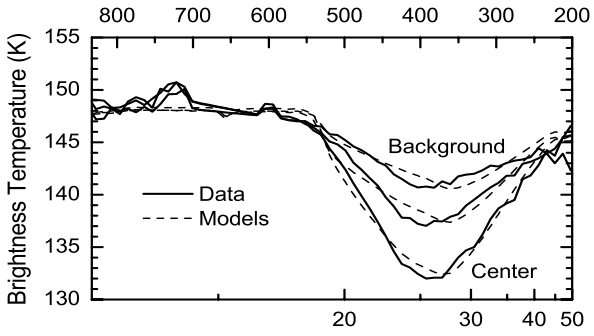

Figure 3

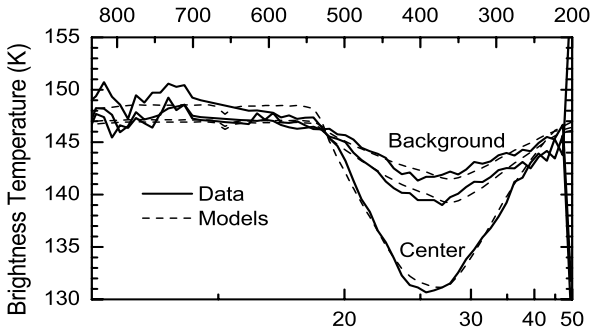

References:

[1] Kieffer *et al.* (1976) *Science, 194*, 1341–1344. [2] Christensen P. R. *et al.* (1992) *JGR, 97*, 7719–7734. [3] Kieffer *et al.* (2000) *JGR, 105*, 9653–9699. [4] Titus *et al.* (2001) *JGR, 106*, 23181–23196. [5] Hansen G. B. (1999) *JGR, 104*, 16471–16486. [6] Forget, F. *et al.* (1998) *Icarus, 131*, 302–316, 1998. [7] Eluszkiewicz, J., and T. N. Titus (2002) *BAAS, 34*, 866. [8] Eluszkiewicz, J. (1993) *Icarus, 103*, 43–48. [9] Hansen, G. B. (2001) *Eos Trans. AGU, 82*, Fall Meet. Suppl., Abstract P12E-09. [10[Christensen P. R. *et al.* (2001) *JGR, 106*, 23823–23871. [11] Hansen, G. B., *BAAS, 34*, 844.